Comparative Application of Multiple Receptor Methods To Identify Aerosol Sources in Northern Vermont

Richard L. Poirot and Paul R. Wishinski

Vermont Department of Environmental Conservation, Building 3 South, 103 South Main Street, Waterbury, Vermont 05671-0402

Philip K. Hopke and Alexander V. Polissar

Department of Chemical Engineering, Clarkson University, Box 5705, Potsdam, New York 13699-5705

ENVIRONMENTAL SCIENCE & TECHNOLOGY

Reprinted from
Volume 35, Number 23, Pages 4622–4636

Environ. Sci. Technol. 2001, 35, 4622–4636

Comparative Application of Multiple Receptor Methods To Identify Aerosol Sources in Northern Vermont

RICHARD L. POIROT AND PAUL R. WISHINSKI

Vermont Department of Environmental Conservation, Building 3 South, 103 South Main Street, Waterbury, Vermont 05671-0402

PHILIP K. HOPKE* AND ALEXANDER V. POLISSAR

Department of Chemical Engineering, Clarkson University, Box 5705, Potsdam, New York 13699-5705

This study applies and compares results of four receptor modeling techniques to a common set of speciated fine particle measurement data collected at a remote site in northwestern Vermont between 1988 and 1995. Two multivariate mathematical models, positive matrix factorization and UNMIX, were applied to the measurement data and identified seven "common" sources that had similar compositions and similar fine mass contributions in both models. Two ensemble backward trajectory techniques, potential source contribution function and residence-time analysis, were also applied to evaluate and interpret the mathematical model results. The trajectory techniques indicate a strong regional character to the upwind locations associated with aerosol contributions from most of the sources identified independently by the mathematical models and help in the interpretation of those results. The process of model comparison provides insights on the strengths and limitations of the individual and combined source attribution techniques. Convergent results among the multiple methods provide a degree of confidence that each of the receptor methods may represent useful tools for future air quality management. Divergent or inconsistent results among the models can help identify limitations of the individual models and of the underlying aerosol and meteorological data sets.

Introduction

Concentrations of fine particles (<2.5 μm) in the ambient air are typically composed of complex mixtures of chemical species, originating from a wide range of natural sources and human activities, distributed over transport distances of tens to thousands of kilometers from their origins. Recent U.S. EPA regulatory programs for fine particles ($PM_{2.5}$) and regional haze have led to a dramatic expansion of ambient measurements of $PM_{2.5}$ mass and chemical composition. Within the next few years, vast amounts of complex new data will become available with associated mandates to use these data to develop efficient emissions control strategies to attain national health-based air quality standards and to reduce regional haze in class I visibility Federal lands.

Receptor models, which attribute pollution to sources through mathematical and/or meteorological interpretation of ambient measurement data, should prove to be useful $PM_{2.5}$ air quality management tools, especially as the quantity and quality of speciated fine particle data increases and as improved methods are developed for treating secondary aerosol formation in these models (*1*). Positive matrix factorization (PMF) (*2*, *3*) and UNMIX (*4*, *5*) are two state-of-the-art multivariate mathematical models that have potential applicability to analysis of speciated fine particle data. At a recent EPA workshop (*6*, *7*), these models were applied to common sets of simulated data (with known sources) and ambient measurement $PM_{2.5}$ data (with unknown sources from the Phoenix area). Several common sources were identified by both models, while other sources were unique to one model or the other.

In the current study, the PMF and UNMIX models are applied to a common set of IMPROVE-like speciated $PM_{2.5}$ data from a remote background site in northwestern Vermont. These model results are compared and further evaluated by two ensemble backward air trajectory techniques: the potential source contribution function (PSCF) (*8*) and residence-time analysis (RTA) (*9*, *10*). Through this "four-way" comparison, some degree of confidence in the usefulness of the different receptor modeling tools applied to this kind of measurement data can be gained in areas where model results are convergent. Conversely, areas where the model results diverged can help identify limitations in the underlying aerosol and meteorological data, the individual modeling approaches, and/or the modeler's interpretation of the results.

Measurement Data

Fine particle measurements were conducted at a remote background site in Underhill, VT (44.53 N, 72.86 W, 400 m elevation), between September 1988 and June 1995 as part of the NESCAUM Regional Particle Monitoring Network (*11*, *12*). Samples were collected on Teflon filters using one of the four modular samplers (module A) routinely employed in the *I*nteragency *M*onitoring of *PRO*tected *V*isual *E*nvironments (IMPROVE) network. Filters were subsequently analyzed at the Crocker Nuclear Laboratory, Univeristy of California, Davis (IMPROVE analytical laboratory) for mass (gravimetric), light absorption (B_{abs}, by laser integrating plate, LIPM), elemental hydrogen (by proton elastic scattering analysis, PESA), and multiple elements with molecular weights ranging from Na through Pb (initially by proton-induced X-ray emission, PIXE, and starting June 1992 by a combination of PIXE and X-ray fluorescence, XRF). The addition of XRF affected the precision and minimum detectable limits for the measured elemental concentrations. Black carbon mass concentrations were calculated using an assumed absorption cross-section for BC aerosol of 25 m^2 g^{-1}. This value is much higher than is typically employed (*13*), but this relationship was obtained between light absorption coefficient and EC at two nearby sites in the NESCAUM network where direct measurements of EC and absorption coefficient were conducted concurrently with the Underhill, VT, measurements (*12*).

Samplers were run 24 h, midnight to midnight, every Wednesday and Saturday (IMPROVE sampling schedule) and also every sixth day (routine EPA PM_{10} sampling schedule), with a resultant data set of 853 samples with 28 measurement variables (see Figure 1). These data include reported con-

* Corresponding author phone: (315)268-3861; fax: (315)268-6654; e-mail: hopkepk@clarkson.edu.

10.1021/es010588p CCC: $20.00
Published on Web 11/02/2001

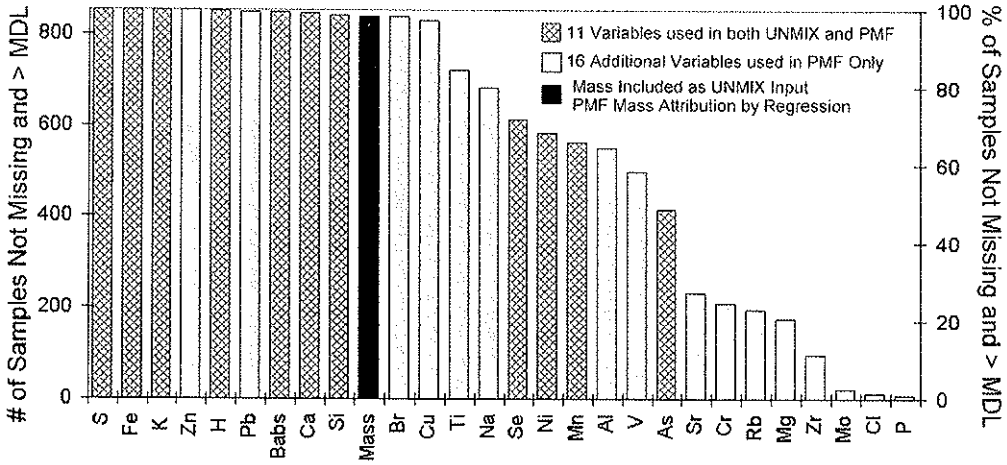

FIGURE 1. Underhill, VT, fine particle variables used as input for UNMIX and PMF model runs.

centrations (in ng/m^3 for all variables except B_{abs}, which is in 10^{-8} m^{-1}) and analytical uncertainties for all concentrations above minimum detection limits (MDL). For attempted measurements below (and above) MDL, a varying MDL is quantified separately for each species and each sample. There are occasional missing data (no reported measurement) for one or more species (most often mass or B_{abs}) in 16 of the 853 daily samples.

Multivariate Models and Methods

Factor analysis, employing a traditional mass balance approach to analysis of multivariate air pollution data, has provided useful insights on sources of gaseous hydrocarbons and speciated aerosols over the past several decades. No assumed knowledge of meteorology or emissions inventories is required, and the model identifies the chemical composition of the identified sources. However, as observed by Henry (*14*), the traditional factor analysis approach is ill-posed and can produce an infinite number of equally "correct" (statistically) but different answers. PMF and UNMIX are refinements of the traditional factor analysis method, which employ different approaches to constrain results to a single unique, physically feasible solution.

In the current study, the PMF and UNMIX models were run semi-independently; PMF run by the Clarkson team and UNMIX run by the Vermont team. The separate modeling groups exchanged preliminary results on several occasions, and both groups made various revisions to their initial modeling approaches over the course of the study. Both groups started with the identical raw data set composed of 853 samples, 28 variables, with associated MDLs and analytical uncertainties. PMF and UNMIX are described in detail elsewhere (*2*–*6*) and are summarized in only general terms here, with emphasis on those differences between the models that resulted in use of different input data by the modelers. Both models, as applied here, are intended to identify the number of discernible sources of influence on the data, the source compositions, the daily contributions from each source to concentrations of fine mass (and of other species used as input to the models), and the associated uncertainties.

One key difference between the models is that PMF allows for weighting of individual data points while UNMIX does not. This weighting option allows inclusion of measurement uncertainties and also provides for innovative treatments of data that are missing or below MDL. Details of the treatment of missing and MDL data points are given by Polissar et al. (*15*). Using this approach, all 27 variables (excluding mass) and all 853 samples were employed as input data for PMF. Mass attribution for the resulting PMF sources was determined by a weighted least-squares regression of the daily source scores vs fine mass.

In UNMIX, which is based on an eigenvalue analysis that precludes individual data point weighting, missing or below MDL data can be treated in one of two general ways: (a) by substituting specific values for missing or below MDL data points or (b) by removing observations or variables for which missing or below MDL data are encountered. In the current study, a combination of these data censoring techniques was employed. Samples with missing data for one or more species were eliminated, reducing the sample size from 853 to 838 observations. An average MDL was calculated for each variable, and values below MDL were replaced with half of this (constant) average MDL for each species. The decision to employ a constant rather than varying MDL resulted from a range of sensitivity tests using alternative "hole-filling" procedures and is explained in more detail by Poirot and Hopke (*16*). The general concern was that the variation in daily (analytical) MDLs appears to be subject to analytical influences, unrelated to air pollution sources (and often leading to no feasible solution in UNMIX sensitivity runs). The number of species was also reduced to 12 UNMIX input variables (including fine mass). The selected species were chosen using a combination of trial and error and the UNMIX overnight option, which allows consideration of multiple numbers and combinations of input variables. The general objective in choosing UNMIX input variables was to maximize the number of input species and resultant sources while producing physically realistic and interpretable results.

The species included as input to PMF and UNMIX and the percentage of observations with reported concentrations above MDL are summarized in Figure 1. Whereas 853 observations × 27 variables were employed as PMF input, less than half as many data points (838 observations of 12 variables) were employed as UNMIX input. Different approaches were also employed in the treatment of analytical uncertainties, MDLs, and mass attribution in the two models.

Ensemble Backward Trajectory Techniques

A set of detailed backward airmass history calculations had been previously calculated for the Underhill, VT, site for 1989–1996—covering about 95% of the dates for which fine particle data and statistical model results were available. These air mass histories were calculated using the CAPITA Monte Carlo model (*17*), with an NGM (*18*) meteorological driver, and include backward trajectory (horizontal and vertical location) positions for each of 10 hypothetical particles released every 2 h from the receptor location and tracked backward in time for 5 days. Details of these air mass

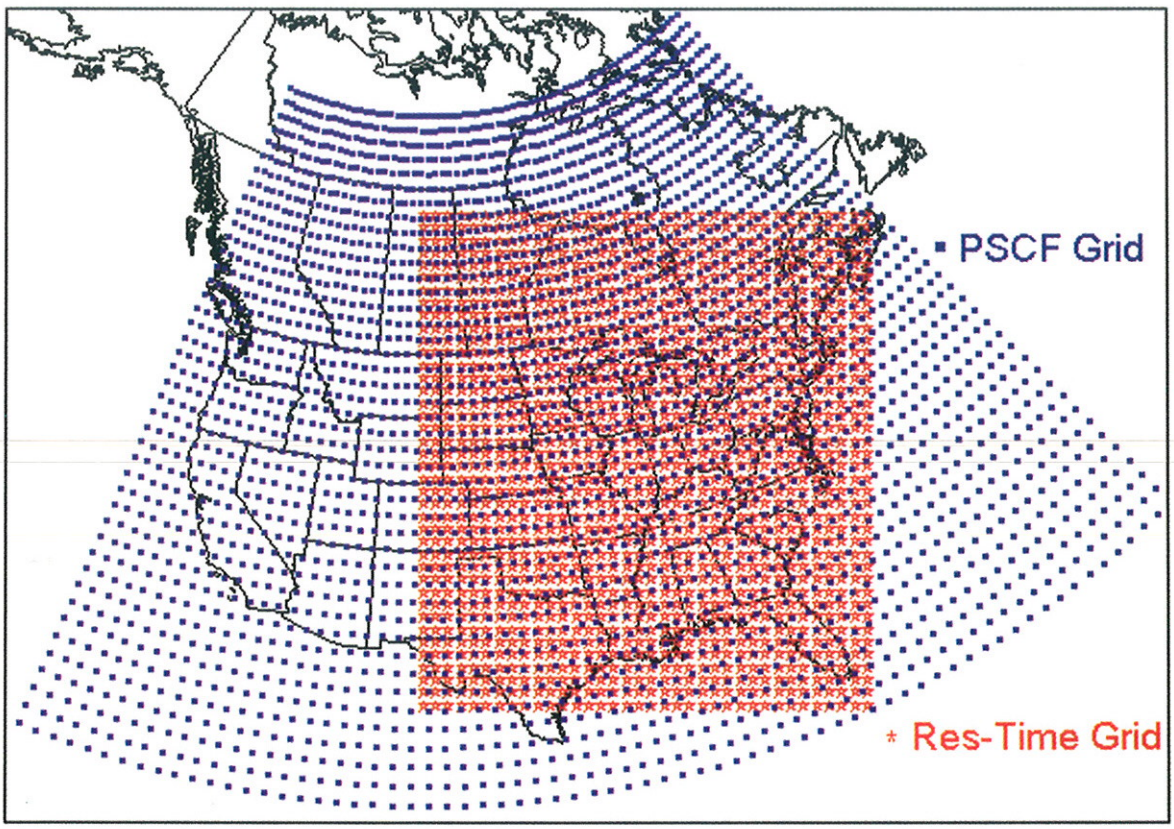

FIGURE 2. PSCF and residence-time analysis trajectory tracking grids.

history calculations are described in detail in Poirot et al. (*20*) and associated references.

In the current study, these CAPITA Monte Carlo trajectories were employed in two ensemble backward trajectory techniques, PSCF and RTA, to evaluate and interpret the results from the multivariate statistical models. As with the mathematical models, the trajectory techniques were applied semi-independently by the Clarkson team (PSCF) and the VT team (RTA). The teams exchanged preliminary results, and both made revisions based on these initial comparisons. The PSCF and RTA techniques are similar in that both apply spatial grids to track and sort the trajectories as a function of metrics derived from the ambient measurement data (in this case, the daily source contributions identified by the mathematical models). The trajectory techniques differ in the domains, the orientations and size of the trajectory tracking grid cells, the metrics employed to attribute trajectories to grid cells, and the metrics calculated from the gridded results.

The PSCF tracking grid covers most of North America with 2966 grid cells of 1° × 1° latitude and longitude. The RTA grid is composed of 1440 squares of 80 × 80 km each covering the eastern United States and southeastern Canada. It may be noted that the RTA squares are equal area (on this stereographic map projection) and are smaller than the PSCF grid cells south of about 60° N latitude. A comparison of the PSCF and RTA grids is displayed in Figure 2.

The individual CAPITA Monte Carlo trajectories were expressed as a series of latitude−longitude coordinates with an initial location 1 h upwind of the receptor location, followed by additional coordinates every 3 h backward in time for 5 days. The trajectory locations are only tracked within the respective domains, such that the average trajectory duration within the RTA domain, for example, is slightly less than 72 h. In the PSCF approach, trajectories are assigned to and temporally disaggregated to the grid cells in their paths by a simple count of trajectory end points within each 1° cell. In the RTA approach, a more computationally intensive technique is employed to disaggregate trajectory subsegments to each grid square and to determine the time (in hours) that each subsegment spends over each grid square.

In the PSCF approach as applied here, a single metric is employed to define the potential source contribution. A count of all trajectory end points in each grid cell for all sampling days at the receptor defines an "all day count". A second count of trajectory end points is determined for a "high day" subset of trajectories (in this case, the highest 40% of daily source contributions for each of the sources identified by the statistical models). The PSCF is defined as the ratio of high day end points to all day end points in each grid cell. A PSCF ratio of <0.4 would indicate that a given grid cell is less likely to be up wind if the source contribution at the receptor was high than it is on an everyday basis, while a ratio of 0.8 would indicate a cell is twice as likely to be upwind on days when the source contribution is high as it is on an everyday basis. Given the large PSCF grid domain and resultant sparse trajectory coverage of the more distant grid cells, an arbitrary weighting function is applied to the PSCF ratios to minimize spurious results that often result from large ratios between small numbers in the most sparsely covered squares. A detailed description of the PSCF methods and results for these data is presented by Polissar et al. (*15*).

In the RTA approach, a variety of different metrics can be applied to the resultant counts of hours in the equal-area grid squares (*21, 22*). One set of RTA metrics, referred to as "concentration-based sorting" begins with the conversion of the gridded trajectory hours to "probability fields" in which, for a given scenario of dates, the "upwind probability" of trajectory location in a given grid square is defined as the fraction of hours in that square as compared to the total hours in all 1440 squares. An everyday probability field is calculated for a scenario of all sample days at the receptor and provides an indication of areas most likely to be upwind of the receptor on a long-term or climatological basis. A high

TABLE 1. Average Underhill, VT, $PM_{2.5}$ Mass Contributions from PMF and UNMIX Models

sources	PMF av mass (ng/m^3)	PMF % reconstructed mass	UNMIX av mass (ng/m^3)	UNMIX % reconstructed mass
MW summer coal	4200	53.13	4643	55.22
woodsmoke	1205	15.24	1314	15.63
MW winter coal	593	7.50	1189	14.14
east coast oil	545	6.90	643	7.65
Can. Mn sources	173	2.19	323	3.84
soil	321	4.06	208	2.47
Canadian smelter	98	1.24	89	1.05
PMF Zn–Pb	581	7.35		
PMF Cu	122	1.54		
PMF Na–S	52	0.65		
PMF salt	15	0.19		
reconstructed mass	7904	100	8408	100

day probability field can be calculated for various definitions of high contributions at the receptor, for example, upper 50th, 75th, or 90th percentile days, etc. The "incremental probability" for a given high day scenario is defined as the difference between the high day and everyday probability fields. An incremental probability field for or an upper 60th percentile definition of high day would differ from the PSCF because the RTA metric is determined by subtraction (the extent to which the high day probability is greater than everyday), while the PSCF metric is determined by division (the fraction of total trajectories passing over a cell that result in high concentration days). Thus, the PSCF indicates the potential for a location to contribute if that area is upwind of the receptor, while the incremental probability reflects the most probable upwind locations if the source contribution is high. A second series of RTA metrics, referred to as "location-based sorting" calculates a summary statistic (mean, median, percentile, etc.) from concentrations (or in this case source contributions) at the receptor for all days with trajectories residing over a each grid square. The summary statistic is weighted by the hours over square of the individual trajectories. As with the PSCF metric, the results from location-based sorting are sensitive to the sparse trajectory coverage of distant grid squares, and a censoring function is applied to exclude calculations in squares with sparse coverage.

Multivariate Model Results

The UNMIX model (run with 838 observations of 12 input variables) identified seven sources. The PMF model (run with 853 observations of 27 input variables) identified 11 sources. The details of the PMF results are presented by Polissar et al. (*15*). The average fine mass source contributions are summarized in Table 1. A comparison of the daily reconstructed fine mass contributions from all the model sources with measured fine mass concentrations is displayed in Figure 3.

It may be noted that both models reproduce the daily mass reasonably well. UNMIX, which included mass as an input variable, reproduced the average and daily mass somewhat more closely (essentially attributing all the mass among the seven identified sources). PMF, which apportioned mass by regression from the daily mass and source scores, leaves some of the mass unexplained by the 11 sources it identified from the 27 nonmass input variables.

The "short" source names indicated in Table 1 are not produced by the models, but rather reflect the best judgment of the modelers. These interpretations are based on the source compositions, time series of the daily source contributions, and subsequent PSCF and RTA results to follow. Note also

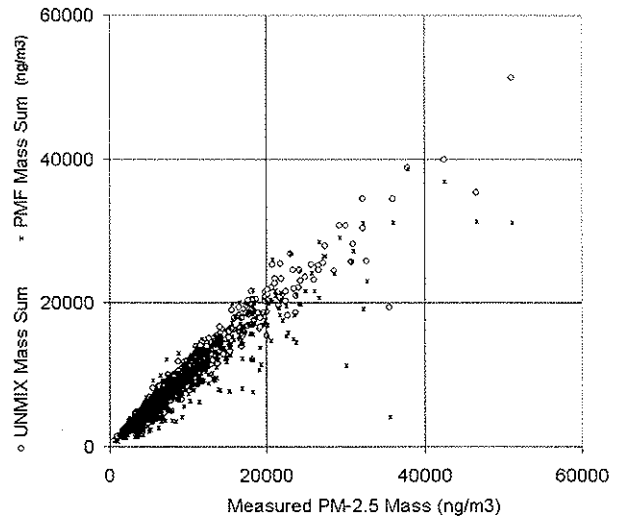

FIGURE 3. Comparison of measured and modeled $PM_{2.5}$ mass values.

that common source names have been applied to "similar" sources that were identified by both PMF and UNMIX models. Again, this judgment of similarity is derived solely from interpretations by the modelers and is based in turn upon comparisons of the source profiles and daily source contributions resulting from the models. These source profiles (for those elements used as common input for both models) and daily source contributions are compared in Figure 4.

Note that in most cases the source profiles are similar, the daily source contributions are well correlated ($R^2 > 0.75$), and the slopes of the daily mass comparisons are generally within 25% of 1:1. Notable exceptions occur for the MW winter coal and the Canadian Mn sources, which have similar composition profiles and highly correlated daily contributions but show substantially higher mass contributions from UNMIX than for PMF—hence the sources are similar, but their mass attribution differs. The soil sources have similar profiles for elements included in both models but show the poorest daily correlation ($R^2 = 0.73$) and a mass contribution from the PMF soil source, which is about 50% higher than from the UNMIX soil source. Despite these discrepancies, the authors feel that it is reasonable to conclude that for the seven sources identified by the UNMIX model, there were similar counterpart sources also identified by PMF.

Average monthly source contributions are displayed in Figure 5 and provide some insights into the selected source names for the similar PMF and UNMIX sources. The largest source—named MW summer coal—accounts for about half the average mass and has a strong summer maxima in both models. The source named MW winter coal displays an opposite seasonality, with a strong winter maxima. These two midwestern sources together account for a majority of the sulfur and selenium in both models, but the summer source has a much higher S:Se ratio, indicative of more efficient sulfur gas to particle conversion chemistry. The sources named east coast oil and woodsmoke also exhibit winter maxima, consistent with seasonal increases in wood and oil fuel combustion. The soil source peaks in spring, while the Canadian Mn and Canadian smelter sources do not exhibit strong seasonal patterns.

Ensemble Trajectory Results

Additional insights into the nature of the identified common PMF and UNMIX sources are provided through a trajectory-based evaluation of the upwind locations associated with high concentrations of these sources. Figures 6 and 7 show comparative results from the PSCF and RTA ensemble trajectory evaluations of the sources named east coast oil

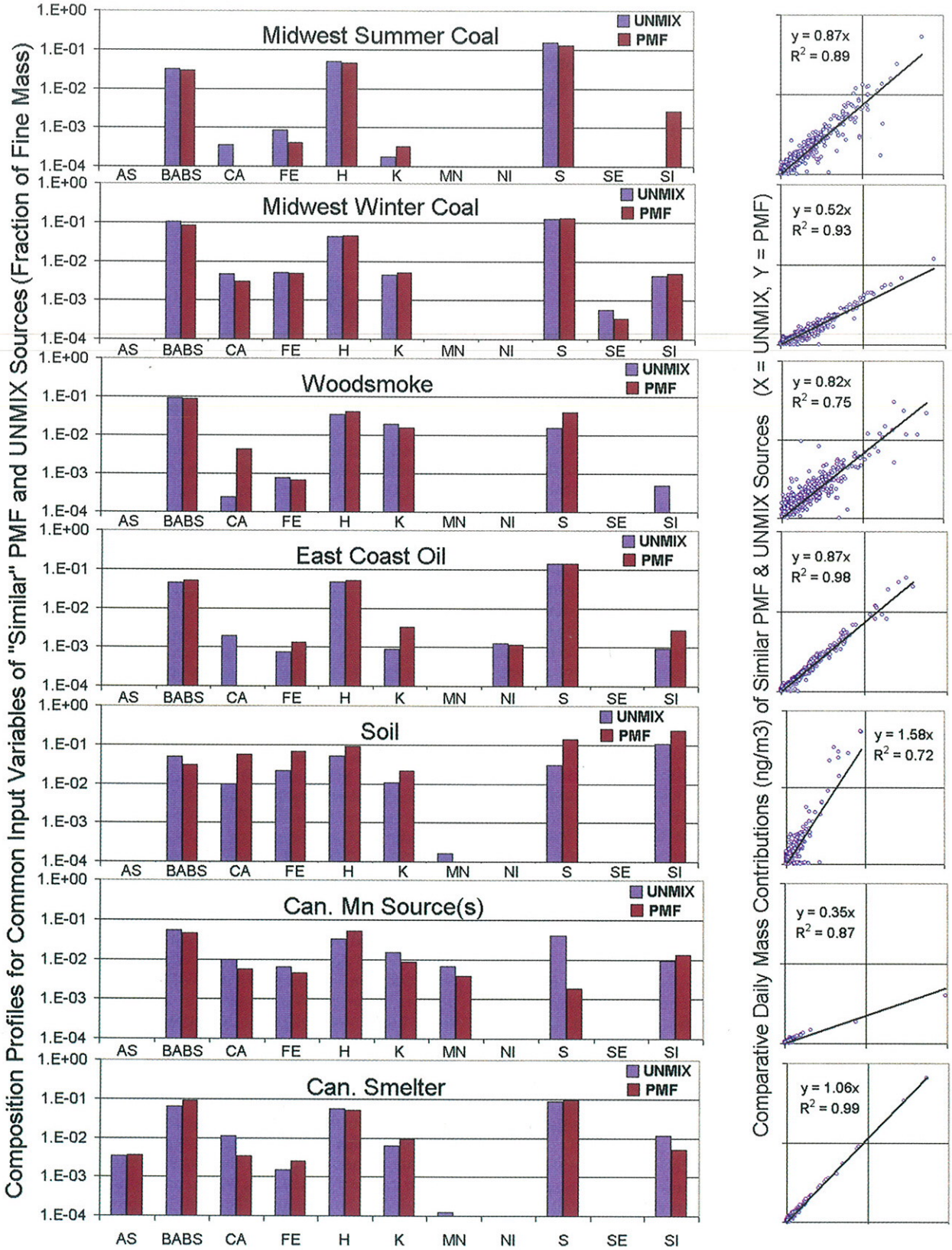

FIGURE 4. Comparison of similar UNMIX and PMF source compositions and daily $PM_{2.5}$ mass contributions.

and Canadian smelter, respectively. Neither of these sources was a large mass contributor in either the PMF or UNMIX results, but the daily source contributions from PMF and UNMIX were in nearly perfect agreement for these two sources, and both have very distinct elemental patterns with a majority of the arsenic (smelter) and nickel (oil) accounted for by these sources. Previous analyses of trace element data from this and rural New England sites (*19, 20*) had indicated that As and Ni were likely to be useful regional tracers for Canadian smelter region and the east coast urban corridor, respectively. Figures 6 and 7 also illustrate some of the similarities in and differences between the PSCF and RTA

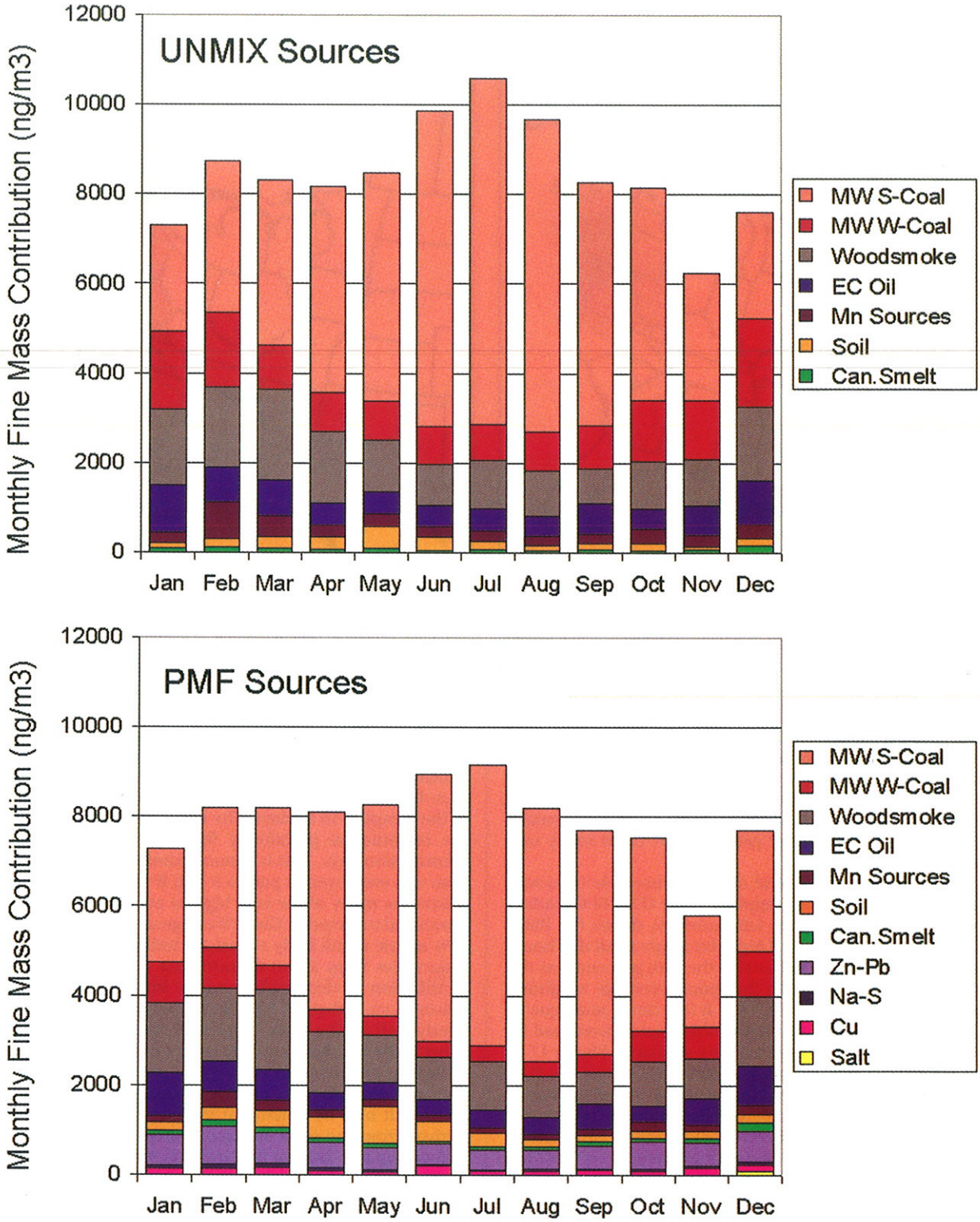

FIGURE 5. Seasonal $PM_{2.5}$ mass contributions from PMF and UNMIX sources.

trajectory tracking methods and in the various metrics used for sorting, aggregating, and displaying the ensemble trajectory results.

Figure 6 employs the same source (the PMF east coast oil source), the same definition of high contribution (the 60th percentile, or highest 40% of the source contribution days), the same metric (ratio of high day to every day), the PSCF sparse coverage weighting function (*15*), and the same common grid domain (the RTA domain) to the plots on both sides of the figure. On the left side, the plotted ratio of high day to everyday is based on trajectory end points in $1° \times 1°$ grid cells, and on the right side, the plotted ratio is based on the ratio of high day to everyday hours in 80×80 km squares. In both cases, the areas with the highest PSCF ratios are clearly centered on the east coast urban corridor. The similarity between the plots indicates that for this particular metric (ratio of high day to every day) there is no substantial difference between the PSCF and RTA trajectory tracking and gridding techniques. The strong agreement between the UNMIX and PMF results, the relatively tight PSCF focus on

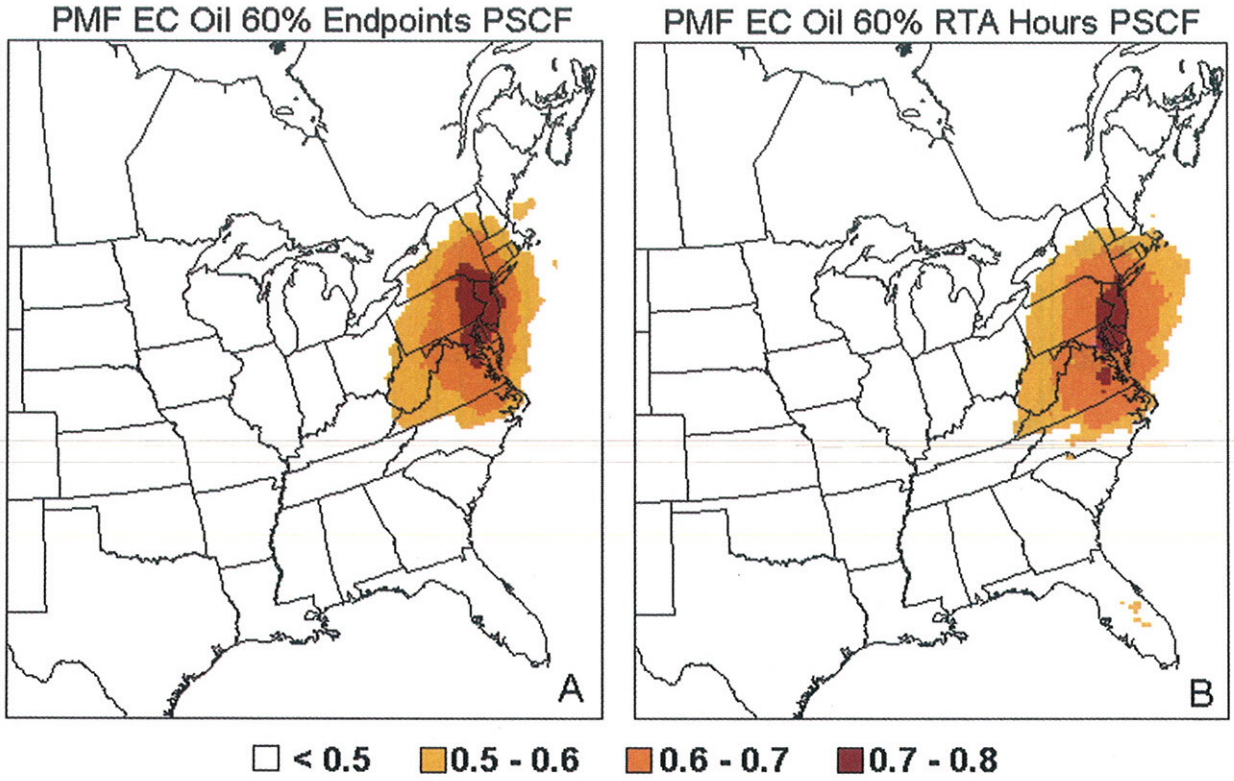

FIGURE 6. Comparison of PSCF and RTA trajectory tracking methods, illustrated by ratio of 60th percentile to everyday for PMF east coast oil source.

the east coast urban corridor, and the high nickel (and vanadium for PMF) are all consistent with emissions from large oil-burning sources (primarily utilities) in that region. The strong winter seasonality in this source contribution (Figure 5) is also consistent with seasonal increases in residual oil combustion for space heating as well as with winter increases in the price of natural gas, which typically results in switching from summer gas to winter oil at many east coast utilities.

Figure 7 compares several different ensemble trajectory techniques and metrics as applied to the UNMIX Canadian smelter source. The upper left panel (A) shows the PSCF calculated from the ratio of high day hours to all day hours using the RTA tracking grid, using the 60th percentile as the definition of high day, with the sparse coverage weighting function from Polissar et al. (*15*). It is a direct analogue to the PSCF for the PMF version of this source presented by Polissar et al. (*15*) and appears very similar to Figure 17 in that reference. The upper right panel (B) shows the RTA incremental probability field for the UNMIX smelter source. Its based on the same (60th percentile) definition of high day as the PSCF but is calculated by subtraction (how much greater is the high day probability than everyday) rather than division (how many times greater is the probability) and thus reflects the frequency with which a location is more likely to be upwind on high source contribution days. The units in panel B (and D) are normalized to the average probability across the whole domain, such that the shaded areas show locations where the incremental probability is 20%, 40%, and 60% (and 80%) higher than average. Compared to the PSCF, the incremental probability plot shows somewhat greater emphasis on the region surrounding the Noranda smelter and less emphasis on areas further west and further south (areas that may be interpreted as having the potential to contribute to the receptor but that are less frequently upwind). The lower left panel (C) of Figure 7 shows the (location-based sorting) RTA calculation of the average contribution of the smelter source as a function of upwind location and (like panel A) also includes the sparse coverage weighting function from Polissar et al. (*15*). The units in panel C are normalized to the average source contribution at the receptor, such that the shaded areas indicate locations from which the average source contribution at the receptor is more than 40%, 60%, and 80% higher than the average contribution at the receptor on all days. The lower right panel (D) shows the incremental probability for the top 10% of source contribution days. This is a more extreme definition of high than was employed in panels A and B—including only one-quarter as many of the very highest contribution days and associated trajectories. Given the large sample size, this upper 10% metric is still fairly robust, including the (120 per day) trajectories from about 80 sampling days. The frequency distribution of this smelter source influence is also quite episodic, such that the highest 10% of the days account for nearly half of the total long-term contribution from the source. The time series for this source indicates a substantial reduction occurring in early 1990, coincident with major revisions to emissions control processes at the Noranda smelter. It may be noted that the plots in panels C and D, derived from the most extreme source contributions, tend to focus most tightly on the Noranda region, while panels A and B include influence from less extreme contribution days and suggest that other sources in other locations may contribute to this source on lower contribution days. An alternative interpretation is that the ensemble trajectory techniques, which are influenced by random or systematic errors in the individual trajectory calculations and/or in the underlying meteorological data, simply produce less definitive results as the definition of high source contribution is reduced.

Figure 8 displays the RTA upwind incremental probability fields for the highest 10% of daily source contributions for the 7 similar sources identified independently by the UNMIX and PMF models. The strong similarities in the incremental probability plots for the similar sources identified by PMF and UNMIX is not surprising, given the strong correlations

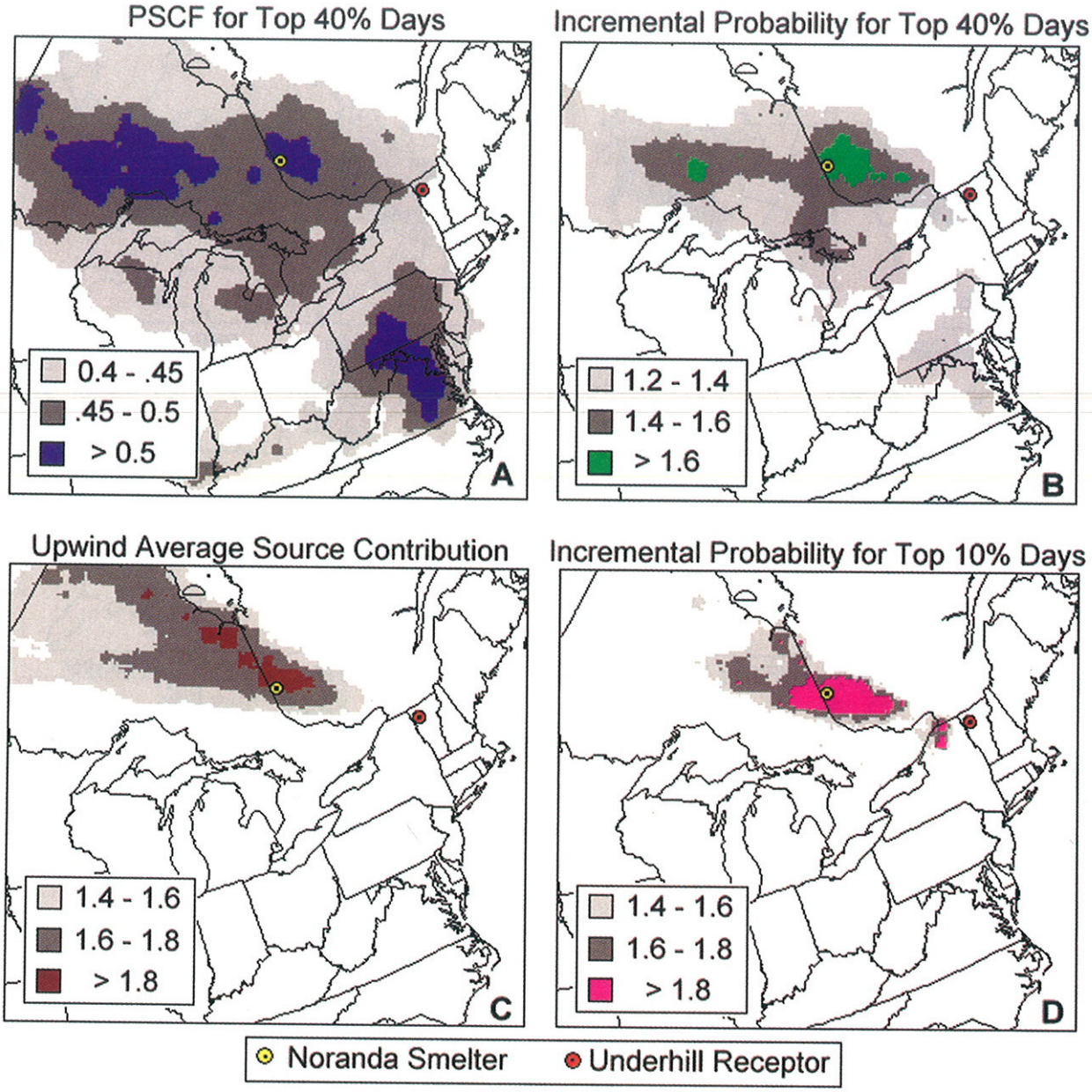

FIGURE 7. Comparison of RTA metrics for UNMIX Canadian smelter source.

between the modeled source contributions indicated in Figure 4. The highest UNMIX source days are also the highest PMF source days. The units employed in this case are 1, 2, and 3 standard deviations (SD) above the mean, where the mean and SD are calculated from each source's incremental probability value across the 1440 square RTA tracking grid.

Figure 9 attempts to summarize the comparative results of the mathematical model and trajectory techniques in a single image. As in Figure 8, it is based on RTA incremental probability fields for the upper 10% of daily source contributions for the seven common sources identified independently by the PMF and UNMIX models. In this case, however, locations are only shaded if the incremental probabilities exceed a high threshold of 1.5 (probability at least 50% greater than average) and only for the source which had the highest upwind probability among all the sources. For clarity a "water mask" is applied to show only locations over land areas. The indicated contributions to fine mass at the VT receptor are based on the average (and range) of the PMF and UNMIX results. While there is some degree of overlap between areas of high probability among adjacent source regions (Figure 8), this overlap is especially strong between the sources identified as MW summer and winter coal, and so an additional isopleth is added to identify the common area where the probability for both these sources was especially high (> 1.7). Generally these two sources are associated with the same upwind source region.

Convergent Results

The sources identified as east coast oil and Canadian smelter are discussed in the previous section. Both sources exhibit strong similarities between the two mathematical models and exhibit strong regional character by the trajectory techniques. Together they account for most of the elemental Ni and As apportioned by PMF and UNMIX but only contribute about 7% (oil) and 1% (smelter) respectively of the average fine mass concentration at the receptor.

The source identified as Canadian Mn sources, which accounts for a majority of elemental Mn but only about 3% of the average fine mass, also appears to have a predominantly Canadian origin. The upwind probability field in Figure 9 suggests a uniquely high probability over the relatively nearby

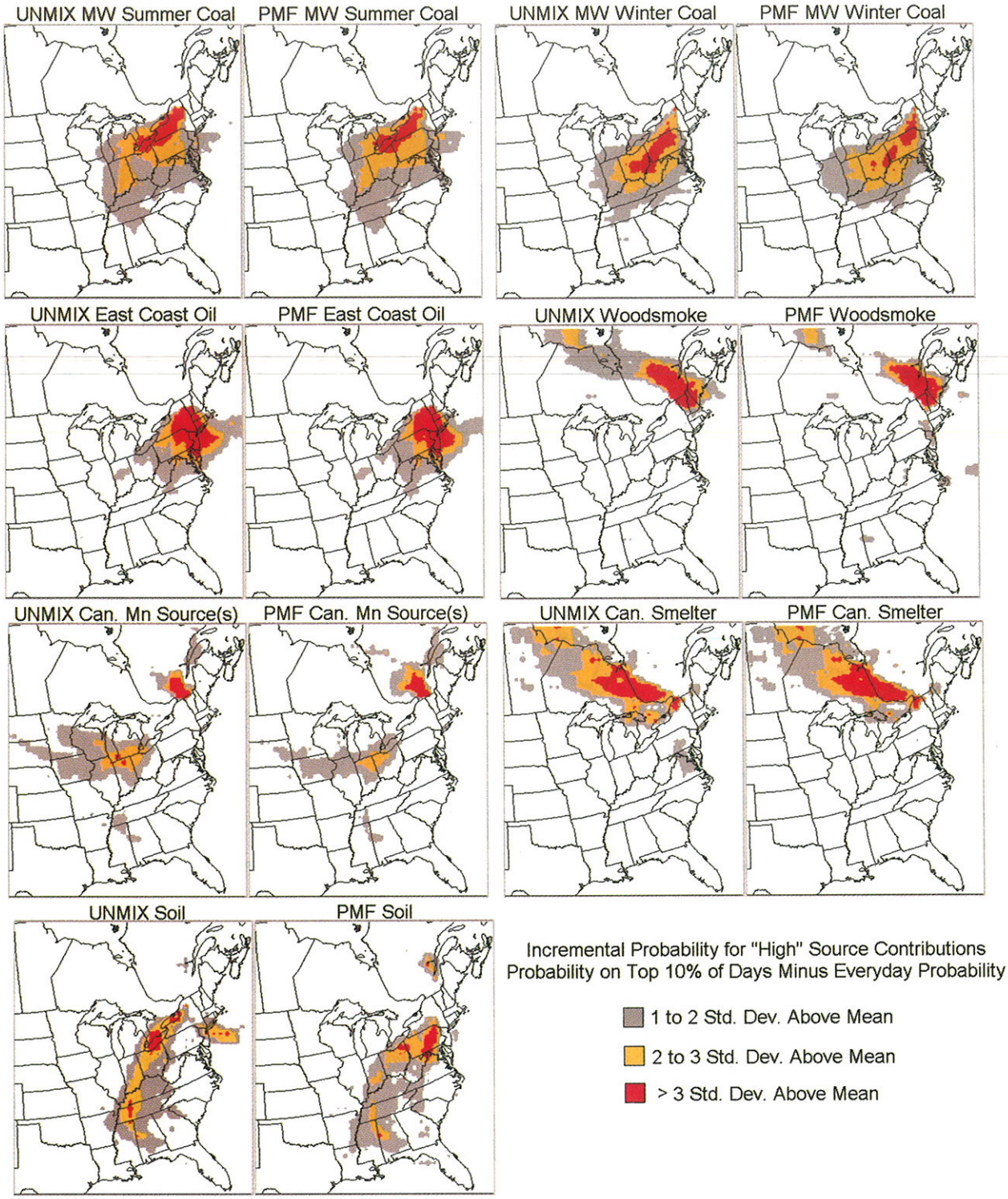

FIGURE 8. RTA incremental probability fields for top 10% of daily UNMIX and PMF source contributions.

Montreal urban area, which is consistent with the influence of Canadian motor vehicles, burning gasoline with a uniquely Canadian Mn additive (methylcyclopentadienyl manganese tricarbonyl, MMT). However, a large Mn alloy production plant just southwest of Montreal in Beauharnois, PQ, may have also been an important Mn source during the first several years of this sampling period (*20*). In the time series for this source presented by Polissar et al. (*15*), there was a substantial drop in the contribution of this source in mid-1991 supporting the role of the smelter as a major contributor to this factor. Also, as may be noted in Figure 8, the Mn source has a second area of relatively high incremental probability along the Great Lakes. Parekh and Husain (*23*) showed that three types of point sources account for most of the noncrustal Mn emissions in the United States. These sources are iron and steel mills, ferro- and sillico-manganese alloy plants, and plants producing Mn metal, synthetic pyrolusite, and Mn chemicals.

The soil source accounts for a large fraction of the crustal elements (Si, Fe, Ca, Al) and about 3% of the fine mass. Its regional location is more ambiguous than suggested in Figure 9 (see Figure 8), as its areas of highest upwind probability overlap with but are much less distinct than those of several other sources. The RTA location-based sorting for the soil

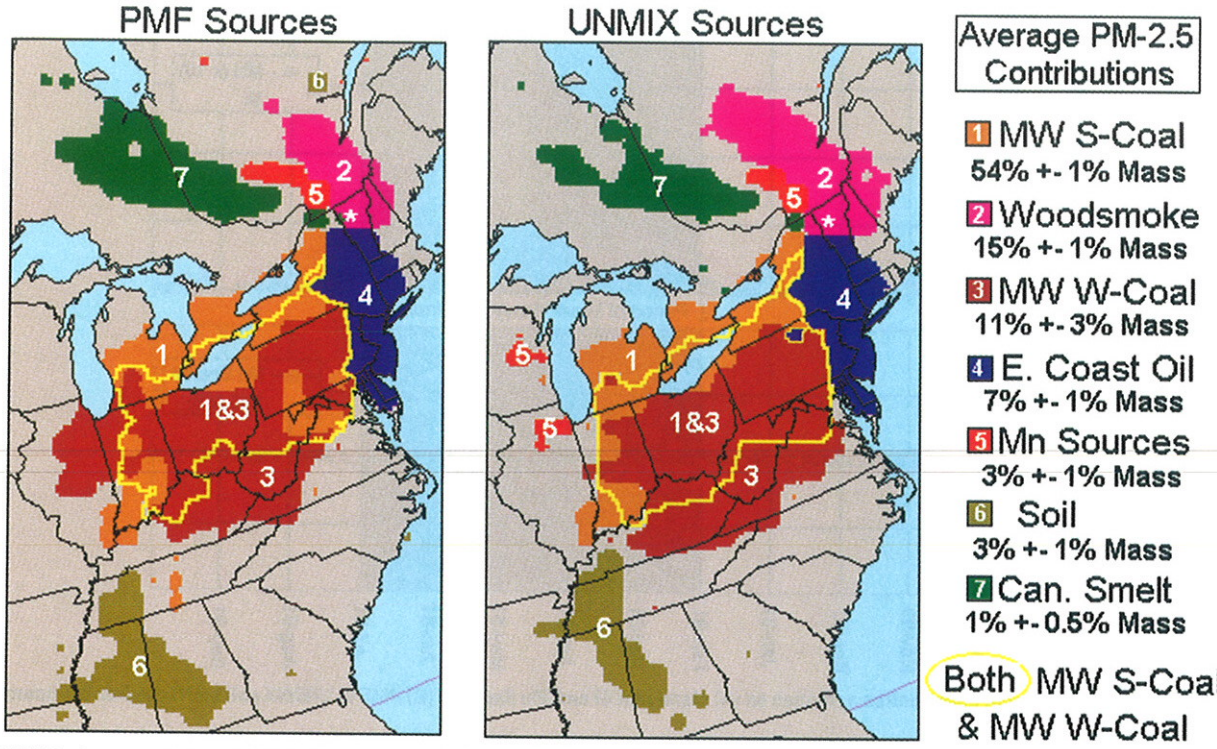

FIGURE 9. Incremental probability fields for top 10% contributions of common PMF and UNMIX sources, showing only locations with highest probability among all sources and average $PM_{2.5}$ mass contributions.

source(s) indicates highest average soil associated with locations in the extreme southwest of the RTA grid. It seems likely that windblown dust emissions from relatively distant arid regions much further to the southwest are significant contributors but that there are also fine soil contributions associated with dry conditions and high wind speeds from a wide range of locations, including occasional, strong local source influences. Unlike other source types, soil emissions (and concentrations) are likely to increase at the highest wind speeds, which makes identification of their origins by these ensemble trajectory techniques problematic. It may also be noted that the incremental probability plots for (top 10% days) for the soil sources in Figures 8 and 9 differ substantially from the PSCF plot (for top 40% days) for the PMF soil source in Polissar et al. (*15*), providing further indication that concentrations of fine soil reaching the receptor result from a wide variety of emissions locations.

The woodsmoke source accounts for a high fraction of the elemental potassium and EC (estimated from B_{abs}) and about 15% of the fine mass. While there were no direct measurements of carbon in this sampling program, the high B_{abs} values suggest a significant elemental carbon content and an indirect estimate of organic matter by the non-sulfate hydrogen (*11, 12*) method (13.75(H-S/4)) suggests that organic carbon compounds may account for about half the mass associated with this source. The woodsmoke time series indicates a general winter maxima (consistent with residential wood burning) but also shows occasional summer spikes, several of which coincide with periods of known forest fire impacts (which were coincidently located in western Quebec). Its incremental probability field is the only one among all the sources that shows high incremental probability in the area immediately surrounding the receptor site, indicating a strong local source influence from residential wood combustion in northern New England and southwestern Quebec.

The sources identified as MW summer coal and MW winter coal together account for more than 90% of the selenium, 80% of the sulfur, and 60% of the fine mass at the receptor. Their incremental probability fields indicate a single, large source region extending from the lower Great Lakes to south of the Ohio River Valley, encompassing the locations of many large, sulfur-emitting utility and industrial sources. The short names MW summer coal and MW winter coal were chosen to reflect the strong, opposite seasonal patterns in these regional influences. As will be discussed in following sections, these sources might best be interpreted as representing the combined primary and secondary aerosol influence from a single midwestern source region, with the so-called winter source approximating the primary aerosol influence and the so-called summer source approximating the secondary aerosol influence from the same region.

Divergent Results

In the preceding sections, the convergent results of the mathematical and models and trajectory techniques have been highlighted. Other aspects of the comparative results are less consistent among the models and help identify limitations in the modeling techniques, problems with the underlying aerosol data, and areas where additional or alternative modeling and measurement approaches may be fruitful.

While the PMF and UNMIX modeling was conducted semi-independently by the Clarkson and VT DEC groups, respectively, these groups exchanged and compared preliminary results on several occasions. Divergent or illogical results led to several modifications in the modeling approaches and/or in the treatment of raw data for model input. Initial conversion of B_{abs} to an estimate of elemental carbon using an assumed absorption efficiency of 10 m^2/g yielded an illogically high mass fraction for a black carbon source from PMF and a poor comparison with UNMIX results. This led to an examination of the historical B_{abs}:EC relationships at nearby concurrent sites and the use of an alternative conversion factor and higher uncertainty weighting more consistent with the measurement data. An initial use of half of the varying detection limit to estimate below detect Se

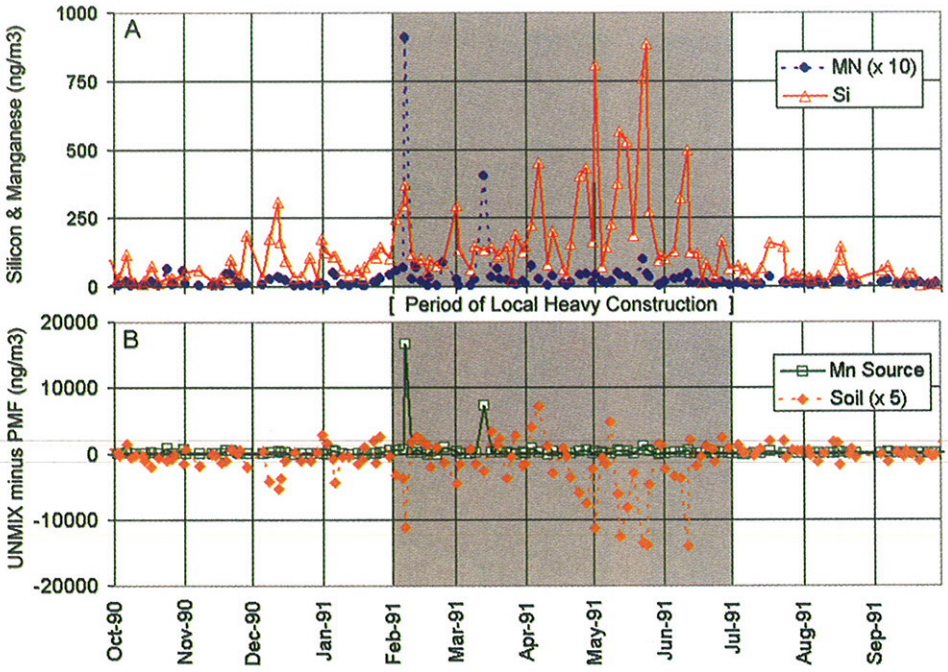

FIGURE 10. Influence of local construction activities on (A) elemental Si and Mn data and (B) PMF vs UNMIX soil and Canadian Mn sources.

concentrations in UNMIX (where no uncertainty weighting is possible) yielded results that compared well with PMF after July 1, 1992 (when the addition of XRF analysis substantially reduced the MDL for Se), but that compared poorly with PMF prior to this date. This led to a closer examination of the trends in detection limits in the data and the subsequent use of half of the (constant) average MDL to estimate below detect values in the UNMIX input data. Thus, a number of divergent preliminary results led to a better understanding of the details of the raw data and to subsequent modifications of the input data for both mathematical models.

For the final results presented here, one clear difference between PMF and UNMIX is in the mass apportionment among the 7 common sources. UNMIX, for which the mass was included as an input variable, apportioned 100% of the mass among the seven sources it identified. PMF, for which the mass was apportioned by regressing the daily source contributions vs the daily fine mass measurements, apportioned 95% of the mass among the 11 identified sources, including 10% of the mass among the four sources that UNMIX did not identify. Thus, the total mass apportioned among the seven common sources was 15% greater for UNMIX than for the PMF counterparts. For four of the common sources, the PMF and UNMIX mass apportionments were within 10% of each other, with the poorest agreement occurring for the soil, Canadian Mn, and MW winter coal sources. The soil and Mn sources are both small, with PMF apportioning 2% of the total reconstructed mass to the Mn source and 4% to soil, while UNMIX reversed these mass fractions to 4% for Mn source and 2% for soil. As indicated in Figure 4, the daily mass contributions from the PMF and UNMIX Mn sources are well correlated ($R^2 = 0.87$), but the PMF mass contribution is only 35% as high as the UNMIX Mn source. The soil sources are less well correlated ($R^2 = 0.72$), and the PMF soil mass contribution is 58% higher than the UNMIX soil mass. A similar "reversal" is indicated in the partial elemental compositions of these sources. The UNMIX Mn source profile includes slightly higher fractions of Ca, Fe, K, and S than the PMF Mn source, while for the soil sources, the PMF source contains higher fractions of these same elements than the UNMIX soil source. Hence it appears that there may have been some "switching" between these two sources in the different mathematical models. Looking more closely at the time series of the raw input data and the source contributions reveals a 5-month period of anomalously high concentrations in the spring of 1991. A laboratory building near the Underhill monitoring site had burned down the preceding winter, and the subsequent reconstruction resulted in a prolonged period of intermittent heavy equipment traffic on the unpaved access road extending from approximately February through June of 1991. During this 5-month period, concentrations of Si (and other crustal elements) and soil source contributions from both the PMF and UNMIX models averaged about 4−5 times higher than during the rest of the 7-yr sampling period. Coincidentally (or not), concentrations of elemental Mn and Canadian Mn source contributions from both the PMF and UNMIX models also averaged about 4−5 times higher than average during this same period. Figure 10 illustrates (top) the high levels of Si and Mn during this 5-month period, with the surrounding year for context. While both species are elevated during the same period, their peak concentrations do not coincide and are only weakly correlated. Peak Mn values occurred on days of moderately high Si and peak Si often occurred on days of moderately high Mn. As indicated in the bottom half of Figure 10, this same 5-month period was also characterized by the greatest divergence between the UNMIX and PMF source contributions for both the Soil and Mn sources. Thus, it appears that the apparent switching between the Mn and Soil sources in the different models may have been at least partially related to the unique data characteristics (and/or unique sources) during this period of local construction. The cause of the elevated Mn concentrations during this period is unknown, but conceivably they were also related to the local construction and traffic activities. Levels of Pb and Br were coincidentally elevated on several of the peak Mn days during this period, suggesting the possibility that one or more of the several heavy vehicles passing along the unpaved access road may have been using fuel with an octane-enhancing Mn additive, thus acting as a temporary but extreme local contributor to the Mn spikes (and as a partial contributor to the local soil emissions as well). In future studies of these data, it might be productive to exclude this period of temporary strong local emissions from the modeling analysis.

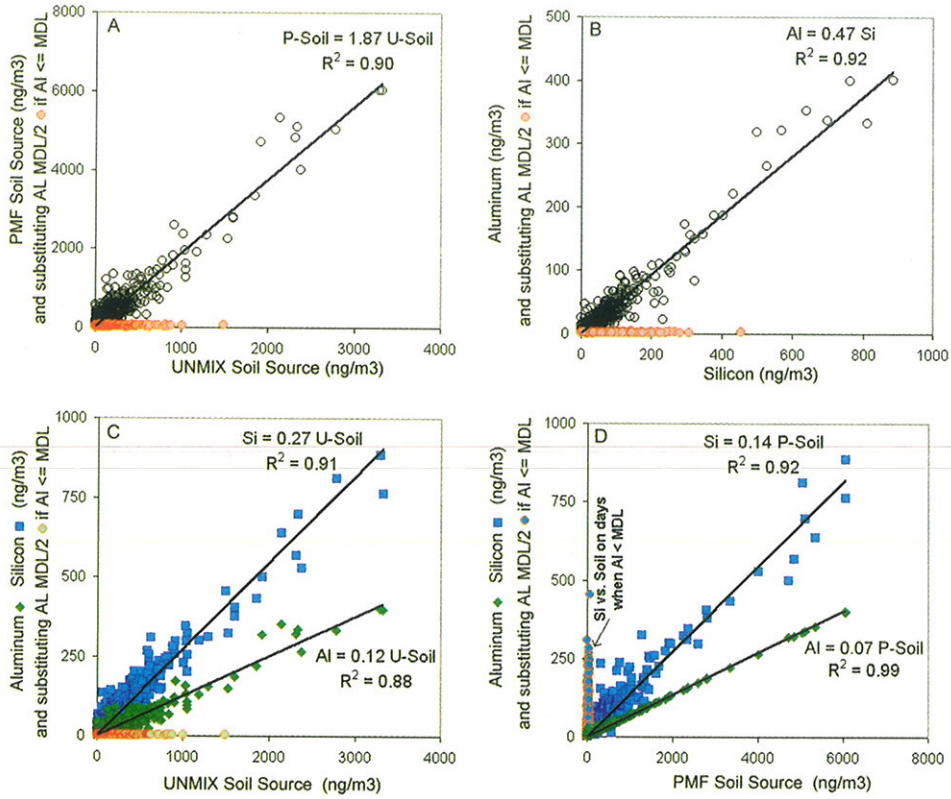

FIGURE 11. Relationships among PMF and UNMIX soil sources and Si and Al data (showing influence of misquantified detection limit for Al).

A second data-related factor which appears to have influenced the different mass apportionment and compositions of the UNMIX and PMF Soil (and possibly other) sources is an apparent problem in the reported minimum detection limits (MDL) for aluminum. Al was below MDL in about one-third of the Underhill samples and was not used as an input variable for UNMIX, as repeated attempts to include it (using several alternative procedures for estimating below MDL Al concentrations) persistently resulted in no feasible solution from the UNMIX model. Al was used as input for the PMF model, where half of the (varying) MDL and an uncertainty of ±0.5 MDL were used to estimate concentrations on below MDL days. Figure 11 compares several aspects of the daily PMF and UNMIX soil source contributions along with relationships to the underlying Al and Si data. Data points for samples where Al was reported as below MDL (and for which half ± half the MDL was used as PMF input) are indicated separately and are excluded from the reported regression lines and equations in Figure 11. When days with Al less than the MDL are excluded from the PMF vs UNMIX Soil contribution comparison, the correlation (R^2) increases from 0.73 (Figure 4) to 0.90 (Figure 11A). In Figure 11B, it can be noted that Al and Si are highly correlated ($R^2 = 0.92$) on days when Al is >MDL, but on days when Al is reported as <MDL (and therefor presumably somewhere between the low reported MDL and zero), Si ranges from low to moderate. Thus, unless there were a source of pure Si that was coincidently present only on days when no other sources of Al were present, it appears as though the Al MDL has been misquantified in the IMPROVE-like data. This problem has subsequently been confirmed by the IMPROVE analytical laboratory (*24*) and does not appear to affect the reported Al concentrations above MDL (as indicated by the strong correlation with Si on the greater than MDL days). Figure 11C indicates that the UNMIX soil source correlates well with Si and with Al on days when Al is greater than the MDL (even though Al was not used as model input), while Figure 11D shows that the PMF Soil correlates nearly perfectly with Al on all days, including days when half the Al MDL was used as an estimate of concentration. PMF soil also correlates well with Si on all days except those when Al less than MDL. Thus, it appears that the PMF soil source has been affected by the misquantified aluminum detection limit in the data. We were unaware of this data artifact at the time the final modeling was conducted but were led to observe it through an evaluation of the divergent results from the PMF and UNMIX models. In future receptor modeling applications, the influence of the data artifact could be minimized or eliminated by avoiding inclusion of Al data as input, constraining input to include only samples where Al is greater than the MDL or using an alternative estimator for Al when MDL levels are indicated (for example, 0.47 × Si might have been a good choice for this data set). This latter estimation technique could also be useful in other applications, such as estimating the reconstructed light extinction from fine soil in implementing the EPA Regional Haze Regulations.

The MW winter coal source also exhibits a distinct difference in the daily mass apportionment between the PMF and UNMIX models, with the UNMIX mass attribution nearly double that of PMF, although the source compositions are quite similar, the daily source contributions are highly correlated, and the trajectory results are very similar. Evaluating these similarities and differences raises the larger question of how the mathematical models treat the influence of secondary aerosols, which is the subject of the following section.

Secondary Sulfate

Receptor models such as PMF and UNMIX require an assumption of (and can only identify sources with) constant, unique source compositions and unique, varying source contributions. These conditions are not well met for sources of a predominantly secondary species like sulfate, which would tend to increase or decrease relative to other primary emissions species (like selenium) as a function of atmospheric

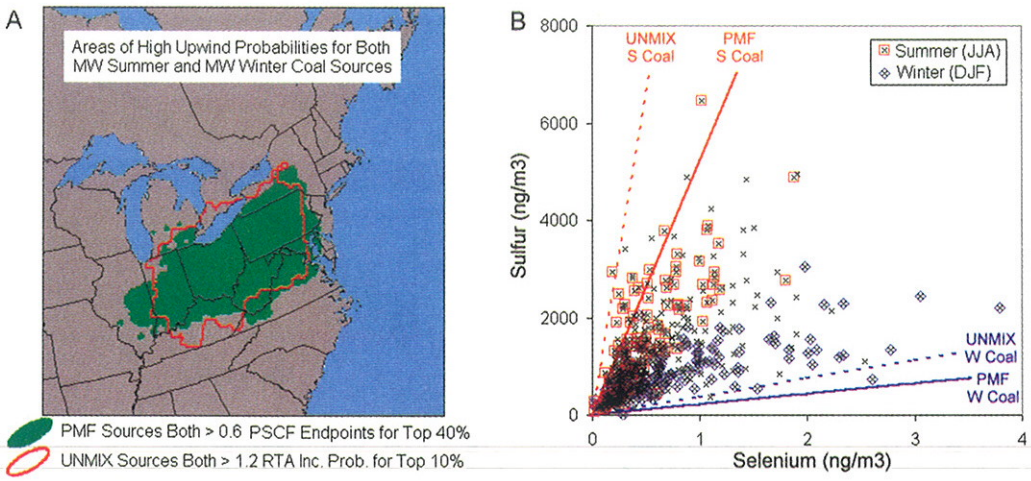

FIGURE 12. Comparative spatial and temporal characteristics and of the combined midwestern sources including (A) common upwind locations for both PMF and UNMIX summer and winter coal sources by both PSCF and RTA trajectory techniques and (B) daily mass and sulfate contributions from combined midwestern sources from PMF vs UNMIX.

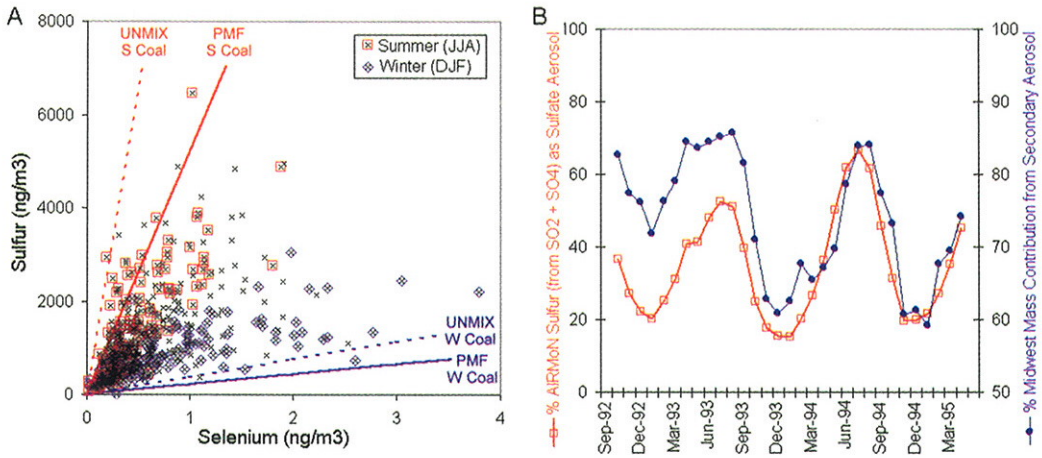

FIGURE 13. Interpretation of the two midwestern sources as approximations of the primary and secondary components of midwestern regional influence, including (A) S:Se ratios in daily Underhill aerosol data and the modeled source compositions and (B) estimates of seasonal variation in secondary aerosol formation, based on combined PMF and UNMIX results, compared with gaseous and aerosol sulfur measurements from the collocated NOAA AIRMoN site.

chemical and meteorological conditions between the sources and receptor. Thus, the virtual source composition (at the receptor) would be highly variable and theoretically not well suited for identification by models such as PMF and UNMIX. Despite the theoretical misfit, however, the identification of two distinct midwestern regional source influence(s) seems to be a relatively robust result and a convergent finding for both mathematical models and both trajectory techniques (and similar results have been noted in recent receptor model applications to IMPROVE data from Brigantine, NJ; *25*). This convergence in the Underhill results is illustrated in Figure 12A, where the green shaded area indicates the area where the PSCF for top 40% days for both the MW summer coal and MW winter coal PMF sources exceed 0.60. The red isopleth shows areas where the RTA incremental probabilities for top 10% days of the UNMIX versions of both of these sources exceed 1.2. Both of these sources, identified by both mathematical models, originate from the same region according to both trajectory techniques.

When the daily mass contributions from the winter and summer midwestern sources from UNMIX are added together and compared with those from PMF (Figure 12B), the resultant regression (PMF = 0.82 UNMIX, $r^2 = 0.94$) shows a better overall fit between the models than the (Figure 4) comparison of the separate summer and winter sources. When the sulfate contributions (expressed in this case as ammonium sulfate or 4.125 S) are compared for the combined midwestern sources, the slope improves to PMF = 0.96 UNMIX. Thus the models' daily apportionments of the total midwestern contributions are in close agreement for fine mass and in very close agreement for sulfate mass.

Additional insight into the nature of the two midwestern sources is provided in the Figure 13A comparison of sulfur and selenium (limited to only above MDL concentrations) in the raw Underhill data. Coal-fired power plants are the largest U.S. emissions sources of both pollutants, with Se released as a primary pollutant (in particle phase or as gaseous emissions which condense relatively quickly to particles) and S emitted primarily in gas phase, followed by relatively slow secondary transformation to particle-phase sulfate compounds. Variations in the rates of secondary transformation result in a highly variable virtual source composition at a distant receptor. This is evident in the wide variations in the S:Se ratios illustrated in Figure 13A, which range from less than 500 to more than 10 000. Combinations of S and Se from summer (June–August) and winter (December–February) are identified by separate red and blue symbols, respectively, and generally fall on opposite sides of an average S:Se ratio of about 2000, although this division is imperfect. There are occasional summer data points with low S:Se ratios and winter days with high ones, while data points from other seasons are scattered throughout the range of the distribution.

The S:Se ratios in the PMF and UNMIX summer and winter MW coal sources are also plotted in Figure 13A. These ratios differ slightly between the models, with the UNMIX sources characterized by higher S:Se, but generally the similar source compositions from both models bound the outer extremes of the S:Se distribution. These extremes can be interpreted as approximations of the contributions of primary (winter coal) and secondary (summer coal) aerosols from a common midwestern source region. More precisely, these extremes reflect the minimal and maximal degrees of secondary midwestern sulfate aerosol formation experienced at the receptor site. The primary component likely includes some small fraction of secondary aerosol, and the secondary component includes some trace amounts of primary aerosols, but they can reasonably be interpreted as approximations (approaching the limits of) primary and secondary midwestern aerosols influencing the receptor. On any given day, the total regional midwestern impact can be described as the linear sum of these two (primary and secondary) source components.

The day to day ratios of these primary and secondary source components provides an indication of the efficiency of sulfate aerosol formation between source and receptor. As the PMF and UNMIX results differ somewhat in the relative split between these components, our best estimate of the primary and secondary aerosol influence is based on an average of the PMF and UNMIX results. When the long-term winter or primary and summer or secondary results are averaged between the two models, 75–80% of the midwestern aerosol is attributed to secondary formation. On a daily basis, the secondary fraction can range from near zero to nearly 100%. On a seasonal basis (expressed as 3-month moving averages in Figure 13B), the secondary aerosol ranges from about 60% in the winter to almost 90% in the summer. For comparison, a separate indicator of the degree of secondary sulfate formation is provided from weekly filter pack measurements of SO_2 and SO_4, which were collected at the Underhill, VT, site as part of the NOAA Atmospheric Integrated Monitoring Network (AIRMoN) (*26*). The AIRMoN sampling commenced in late August 1992, providing a period of nearly 3 yr of concurrent sampling with the NESCAUM aerosol measurements. From these weekly filter pack data, an indicator of the degree of secondary sulfate production can be estimated by calculating the fraction of total sulfur (from both SO_2 and SO_4), which is contributed by SO_4. This percent sulfate metric is displayed in Figure 13B, expressed in the same 3-month moving average temporal units as the combined PMF and UNMIX-derived estimates of secondary midwestern aerosol contributions. These two independent indicators of secondary aerosol formation both show a strong and similar degree of seasonal variation, providing added confidence that the two midwestern sources identified by PMF and UNMIX do represent reasonable approximations of the primary and secondary aerosol contributions from a single, common source region. Thus the models appear to have addressed a highly variable virtual source composition by splitting it into two components, each with a constant composition but mixed together in different proportions on different days).

Concluding Comments

Receptor models, of both the mathematical (PMF and UNMIX) and trajectory (PSCF and RTA) types promise to be helpful tools for source attribution for $PM_{2.5}$ and regional haze. However, each of these techniques also has limitations, and none of them should be considered a "stand alone" technique. Both the mathematical and trajectory approaches are limited by the inherent "resolving power" or detail of the input (aerosol species or meteorological) data. Both techniques are sensitive to systematic errors or biases in the input data, including those introduced by the modelers, such as in the treatment of variables which are missing or below detection limits. The mathematical techniques objectively identify sources of influence on the data, but a good deal of subjective judgment is inevitably required in the interpretation of what these identified sources actually represent. The ensemble trajectory techniques produce only qualitative indications of predominant transport patterns and can be highly sensitive to the subjective metrics calculated from the gridded results. In the absence of very costly chemical tracer experiments, there are virtually no methods to evaluate the performance of any of these mathematical or trajectory receptor models.

For these reasons, we recommend the application and intercomparison of multiple receptor techniques as a useful future approach for improving the understanding of source–receptor relationships for fine particles, for improving the confidence in the individual model results, and for developing a better understanding of the underlying aerosol data. In the current study, the trajectory techniques proved invaluable in the interpretation of mathematical model results. The independent application of separate mathematical and trajectory techniques by the Clarkson and VT groups followed by subsequent exchange and comparison of preliminary results led to refinements in the individual modeling approaches, provided insights into limitations and errors associated with the aerosol measurement data, and improved our collective confidence in the final results.

Literature Cited

(1) Hopke, P. K. Receptor modeling for air quality management. In *Proceedings: AWMA/AGU Specialty Conference on Visual Air Quality: Aerosols and Global Radiation Balance*; Bartlett, NH, 1997.

(2) Paatero, P.; Tapper, U. *Environmetrics* **1994**, *5*, 111–126.

(3) Paatero, P. *User's Guide for Positive Matrix Factorization Programs PMF2 and PMF3*; 1998.

(4) Henry, R. C.; Lewis, C. W.; Collins, J. F. *Environ. Sci. Technol.* **1994**, *28*, 823–832.

(5) Henry, R. C. *UNMIX Version 2 Manual*; Prepared for the U.S. Environmental Protection Agency; 2000.

(6) Willis, R. D. *Workshop on UNMIX and PMF as Applied to $PM_{2.5}$*; EPA/600/A-00/48; 2000.

(7) Eberly, S. I.; Coutant, B. W.; Lewis, C. W. *EPA Workshop on Source Apportionment Tools UNMIX and PMF As Applied to PM2.5 Synthetic Data Set Generation*; 2000.

(8) Zeng, Y.; Hopke, P. K. *Atmos. Environ.* **1989**, *23*, 1499–1509.

(9) Ashbaugh, L. L.; Malm, W. C.; Sadeh, W. Z. A methodology for establishing the probability of the origin of air masses containing high pollutant concentrations. Presented at the 76th Annual APCA Meetings, Atlanta, GA, 1983.

(10) Poirot, R L.; Wishinski, P. R. *Atmos. Environ.* **1986**, *20*, 1457–1469.

(11) Flocchini, R. G.; Cahill, T. A.; Eldred, R. A.; Feeney, P. J. Particulate sampling in the Northeast: a description of the NESCAUM network. *Transactions: A&WMA/EPA Specialty Conference on Visibility and Fine Particles*; Mathai, C. V., Ed.; Estes Park, CO, 1990.

(12) Poirot, R. L.; Galvin, P. J.; Gordon, N.; Quan, S.; Van Arsdale, A.; Flocchini, R. G. *Annual and Seasonal Fine Particle Composition in the Northeast: Second Year Results from the NESCAUM Monitoring Network*; No. 91-49.1; 84th Annual A&WMA Meeting, Vancouver, Canada, 1991.

(13) Horvath, H. *Atmos. Environ.* **1993**, *27A*, 293–317.

(14) Henry, R. C. *Atmos. Environ.* **1987**, *21*, 1815–1820.

(15) Polissar, A. V.; Hopke, P. K.; Poirot, R. L. *Environ. Sci. Technol.* **2001**, *35*, 4604–4621.

(16) Poirot, R. L.; Hopke, P. K. The Potential Influence of Data Artifacts on Receptor Model Results. Presented at the Air & Waste Management Association/EPA Meeting on Measurement of Toxic Air Pollutants, Research Triangle Park, NC, September 18–20, 2000.

(17) Schichtel, B. A.; Husar, R. B. *J. Air Waste Manage. Assoc.* **1996**, *47*, 331–343.

(18) Rolph, G D. *NGM Archive TD-6140, January 1991–June 1996*; Prepared for National Climatic Data Center (NCDC), 1996.

(19) Wishinski, P. R.; Poirot, G.; Keeler, R.; Artz, P.; Galvin, R.; Flocchini, R.; Husar, B.; Schichtel, VanArsdale, A. Transboundary Implications of Visibility-Impairing Aerosols in the Northeastern United States, Part 1: Air Trajectory Assessment of the NES-CAUM Aerosol Data. Presented at AGU/CGU Spring Meeting, Montreal, Canada, 1992.
(20) Poirot, R.; Wishinski, P.; Schichtel, B.; Girton, P. *Air Trajectory Pollution Climatology for the Lake Champlain Basin*; Manley, T., Manley, P., Eds.; AGU Water Monograph on Lake Champlain Research and Implementation; American Geophysical Union: Washington, DC, 1999.
(21) Wishinski, P. R.; Poirot R. L. *Long-Term Ozone Trajectory Climatology for the Eastern US, Part I: Methods*; 98-A613; 91st Annual A&WMA Meeting, San Diego, CA, 1998.
(22) Poirot, R. L.; Wishinski, P. R. *Long-Term Ozone Trajectory Climatology for the Eastern US, Part II: Results*; 98-A615; 91st Annual A&WMA Meeting, San Diego, CA, 1998.
(23) Parekh, P.; Hussain, L. *Atmos. Environ.* **1990**, *24A*, 415−421.
(24) Eldred, R. A. Personal communication, 2000.
(25) Lee, J. H. Personal communication, 2001.
(26) NOAA Air Resources Laboratory Atmospheric Integrated Monitoring Network (AIRMoN). http://gus.arlhq.noaa.gov/research/programs/airmon.html, 2001.

Received for review January 29, 2001. Revised manuscript received September 25, 2001. Accepted September 27, 2001.

ES010588P

Additions and Corrections

2001, Volume 35, Pages 4622−4636

Richard L. Poirot, Paul R. Wishinski, Philip K. Hopke*, and Alexander V. Polissar: Comparative Application of Multiple Receptor Methods To Identify Aerosol Sources in Northern Vermont

Page 4634. Figure 12B was incorrect. This is the correct version of the figure. Panel A and the caption are correct as published.

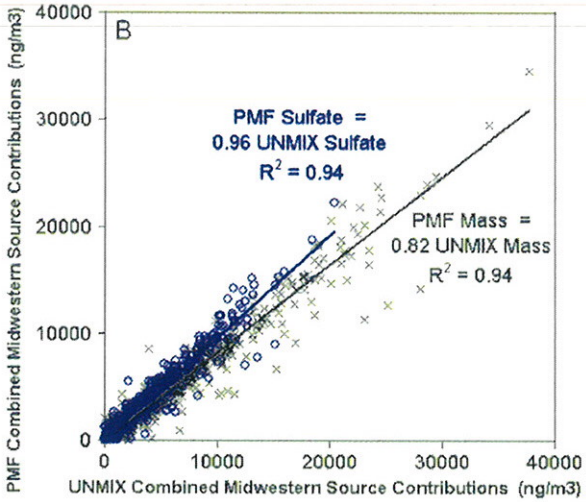

ES011442T

10.1021/es011442t

(2) Vidal B., F.; Ollero, P. *Environ. Sci. Technol.* **2001**, *35*, 2792−2796.
(3) Ravindra, P. V.; Rao, D. P.; Rao, M. S. *Ind. Eng. Chem. Res.* **1997**, *36*, 5125−5132.
(4) Kumar, S. S.; Govindarao, V. M. H.; Chandas, M. *J. Chem. Technol. Biotechnol.* **1996**, *67*, 39−52.
(5) Kumar, S. S.; Govindarao, V. M. H.; Chandas, M. *J. Chem. Technol. Biotechnol.* **1997**, *69*, 209−225.
(6) Vladea, R. V.; Hinrichs, N.; Hudgins, R. R.; Suppiah, S.; Silveston, P. L. *Energy Fuels* **1997**, *11*, 277−283.
(7) Shaikhl, A. A.; Zaidi, S. M. J. *React. Kinet. Catal. Lett*, **1998**, *64* (2), 343−349.
(8) Govindarao, V. M. H.; Gopalakrishna, K. V. *Ind. Eng. Chem. Res.* **1995**, *34*, 2258−2271.
(9) Uttam, R.; Datta, S.; Utpal, R.; Mukherjee, N. C. *IE(I) J.-CH* **1996**, *76*, 29−33.
(10) Ermakov, A. N.; Poskrebyshev, G. A.; Purmal, A. P. *Kinet. Catal.* **1997**, *38* (3), 295−308.
(11) Clarke, A. G.; Radojevic, M. *Atmos. Environ.* **1983**, *17* (3), 617−624.
(12) Beilke, S.; Lamb, D.; Miller, J. *Atmos. Environ.* **1975**, *9*, 1083−1090.

F. Vidal B.* and Pedro Ollero

Department of Chemical and Environmental Engineering
University of Sevilla
Camino de los Descubrimientos s/n
41092 Sevilla, Spain

ES011422R